Investigation of mode coupling in a microdisk resonator for realizing directional emission

Yue-De Yang, Shi-Jiang Wang, and Yong-Zhen Huang

State Key Laboratory on Integrated Optoelectronics, Institute of Semiconductors, Chinese Academy of Sciences, PO Box 912, Beijing 100083, China

yzhuang@semi.ac.cn

Abstract: Mode coupling between the whispering-gallery modes (WGMs) is numerically investigated for a two-dimensional microdisk resonator with an output waveguide. The equilateral-polygonal shaped mode patterns can be constructed by mode coupling in the microdisk, and the coupled modes can still keep high quality factors (Q factors). For a microdisk with a diameter of 4.5 μm and a refractive index of 3.2 connected to a 0.6-μm-wide output waveguide, the coupled mode at the wavelength of 1490 nm has a Q factor in the order of 10^4, which is ten times larger than those of the uncoupled WGMs, and the output efficiency defined as the ratio of the energy flux confined in the output waveguide to the total radiation energy flux is about 0.65. The mode coupling can be used to realize high efficiency directional-emission microdisk lasers.

OCIS codes: (140.3945) microcavities; (140.4780) optical resonators; (140.5960) semiconductor lasers.

References and links

1. S. L. McCall, A. F. J. Levi, R. E. Slusher, S. J. Pearton, and R. A. Logan, "Whispering-gallery mode microdisk lasers," Appl. Phys. Lett. **60**(3), 289–291 (1992).
2. C. Gmachl, F. Capasso, E. E. Narimanov, J. U. Nöckel, A. D. Stone, J. Faist, D. L. Sivco, and A. Y. Cho, "High-power directional emission from microlasers with chaotic resonators," Science **280**(5369), 1556–1564 (1998).
3. G. D. Chern, H. E. Tureci, A. D. Stone, R. K. Chang, M. Kneissl, and N. M. Johnson, "Unidirectional lasing from InGaN multiple-quantum-well spiral-shaped micropillars," Appl. Phys. Lett. **83**(9), 1710–1712 (2003).
4. S. K. Kim, S. H. Kim, G. H. Kim, H. G. Park, D. J. Shin, and Y. H. Lee, "Highly directional emission from few-micron-size elliptical microdisks," Appl. Phys. Lett. **84**(6), 861–863 (2004).
5. S. V. Boriskina, T. M. Benson, P. Sewell, and A. I. Nosich, "Directional emission, increased free spectral range, and mode Q-factors of 2-D wavelength-scale optical microcavity structures," IEEE J. Sel. Top. Quantum Electron. **12**, 1175–1182 (2006).
6. S. J. Choi, K. Djordjev, S. J. Choi, and P. D. Dapkus, "Microdisk lasers vertically coupled to output waveguides," IEEE Photon. Technol. Lett. **15**(10), 1330–1332 (2003).
7. J. Van Campenhout, P. Rojo Romeo, P. Regreny, C. Seassal, D. Van Thourhout, S. Verstuyft, L. Di Cioccio, J. M. Fedeli, C. Lagahe, and R. Baets, "Electrically pumped InP-based microdisk lasers integrated with a nanophotonic silicon-on-insulator waveguide circuit," Opt. Express **15**(11), 6744–6749 (2007).
8. Y. Baryshnikov, P. Heider, W. Parz, and V. Zharnitsky, "Whispering gallery modes inside asymmetric resonant cavities," Phys. Rev. Lett. **93**(13), 133902 (2004).
9. S. Y. Lee, S. Rim, J. W. Ryu, T. Y. Kwon, M. Choi, and C. M. Kim, "Quasiscarred resonances in a spiral-shaped microcavity," Phys. Rev. Lett. **93**(16), 164102 (2004).
10. J. Wiersig, and M. Hentschel, "Unidirectional light emission from high-Q modes in optical microcavities," Phys. Rev. A **73**(3), 031802 (2006).
11. Y. Z. Huang, Y. H. Hu, Q. Chen, S. J. Wang, Y. Du, and Z. C. Fan, "Room-Temperature Continuous-Wave Electrically Injected InP–GaInAsP Equilateral-Triangle-Resonator Lasers," IEEE Photon. Technol. Lett. **19**(13), 963–965 (2007).
12. Y. Z. Huang, K. J. Che, Y. D. Yang, S. J. Wang, Y. Du, and Z. C. Fan, "Directional emission InP/GaInAsP square-resonator microlasers," Opt. Lett. **33**(19), 2170–2172 (2008).
13. M. Hentschel, and K. Richter, "Quantum chaos in optical systems: the annular billiard," Phys. Rev. E Stat. Nonlin. Soft Matter Phys. **66**(5 Pt 2), 056207 (2002).
14. A. Taflove, and S. C. Hagness, *Computational Electrodynamics: The Finite-Difference Time-Domain Method*. (Boston: Artech House, 2005).
15. W. H. Guo, W. J. Li, and Y. Z. Huang, "Computation of resonator frequencies and quality factors of cavities by FDTD technique and padé approximation," IEEE Microwave. Wireless Compon. Lett. **11**(5), 223–225 (2001).

#115046 - $15.00 USD Received 31 Jul 2009; revised 9 Oct 2009; accepted 23 Nov 2009; published 1 Dec 2009

16. Y. Z. Huang, S. J. Wang, Y. D. Yang, J. L. Xiao, Y. H. Hu, and Y. Du, "Optical bistability in InP/GaInAsP equilateral-triangle-resonator microlasers," Opt. Lett. **34**(12), 1852–1854 (2009).
17. M. Fujita, and T. Baba, "Microgear laser," Appl. Phys. Lett. **80**(12), 2051–2053 (2002).
18. Y. D. Yang, Y. Z. Huang, and S. J. Wang, "Mode analysis for equilateral–triangle -resonator microlasers with metal confinement layers," IEEE J. Quantum Electron. in press.
19. Y. D. Yang, Y. Z. Huang, and Q. Chen, "High-Q TM whispering-gallery modes in three-dimensional microcylinders," Phys. Rev. A **75**(1), 013817 (2007).

1. Introduction

Semiconductor microdisk lasers [1] are suitable for realizing ultra-low-threshold operation due to the ultra-small volumes and high Q factors. However, the output power and directional emission in microdisk lasers are greatly limited by the symmetry of the microdisk, and many works are focused to get directional emission microlasers. Deformed microdisk resonators were applied to fabricate directional emission semiconductor microlasers [2–5], and microdisk lasers vertically coupled to a bus waveguide were demonstrated by thermally wafer bonded technique [6,7]. Furthermore, confined modes with different mode field patterns were investigated theoretically for realizing directional emission in deformed microdisks [8,9], and unidirectional light emission by coupling a low-Q mode to a high-Q mode was simulated for microdisks with a hole [10]. Recently, room temperature operation electrically injected InGaAsP/InP triangular and square microlasers were fabricated with a connected output waveguide [11,12].

In the triangle and square microresonators, the mode field patterns along the perimeter of the resonators are modulated by the longitudinal and the transverse mode field distributions with the envelope of transverse mode distribution. So we can connect an output waveguide to the resonator at the position with weak field distribution, and have high Q confined modes for realizing direction emission. However, the mode field pattern along the perimeter of a perfect microdisk is only the longitudinal field distribution with a uniform envelope for whispering-gallery modes (WGMs). Connecting an output waveguide to the microdisk, we usually expect that the Q factors of the WGMs are greatly reduced due to strong couple to the output waveguide. In this paper, we report that the mode coupling can happen between two WGMs with near mode wavelengths, as an output waveguide is connected to the microdisk. The output waveguide destroys the symmetry of the microdisk and results in the mode coupling. The coupled modes have equilateral-polygonal shaped mode patterns, and can have high Q factors with high output coupling efficiency to the output waveguide.

2. Mode superposition in a perfect microdisk

For a two dimensional (2D) microdisk with a radius of R and a refractive index of n surrounded by air, the field distribution of the confined WGMs can be expressed by the Bessel function $J_v(x)$ and the first kind Hankel function $H_v^{(1)}(x)$, and the mode wavelengths and Q factors of the WGMs can be calculated by the following eigenvalue equation [13]

$$J_v(nk_0R)H_v^{(1)'}(k_0R) = \eta J_v'(nk_0R)H_v^{(1)}(k_0R), \qquad (1)$$

where k0 is wavenumber in air, η equals to n and 1/n for TMv,m and TEv,m WGMs, respectively, and v and m are angular and radial mode numbers. The mode wavelengths and Q factors of $TM_{18,3}$ and $TM_{15,4}$ modes obtained from Eq. (1) are 1489.5 and 1489.4 nm, and 6.05×10^7 and 8.29×10^4, respectively, for the 2D microdisk with the diameter of 4.5 μm and the refractive index of 3.2 surrounded by air. When two WGMs have nearly the same mode wavelength, the mode superposition of them can result in equilateral-polygonal mode patterns. The side number of the equilateral polygon is equal to the difference between the angular mode numbers of the two WGMs. The triangular shaped field patterns constructed by the superposition of $TM_{18,3}$ and $TM_{15,4}$ with the same amplitude and the phase differences of π and 0 are plotted in Figs. 1(a) and 1(b), respectively, for symmetric modes relative to the horizontal middle line, i.e., the x-axis. However, the phase difference between the two WGMs is not a constant value as they do not have exactly the same mode wavelength, so the superposition mode distributions are not invariable. Furthermore, mode superposition only

describes the superposition of the field distributions, and the two modes still have different wavelengths and Q factors.

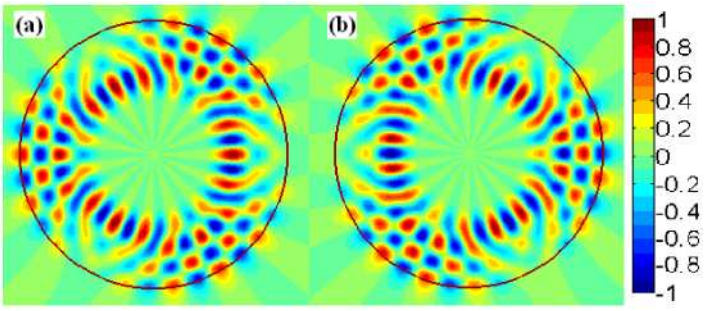

Fig. 1. The triangular shaped mode field patterns constructed by the superposition of $TM_{18,3}$ and $TM_{15,4}$ with phase difference of (a) π and (b) 0 in the perfect microdisk

3. Mode coupling for TM modes in a microdisk with an output waveguide

The mode coupling between the WGMs with different angular mode number is forbidden in a perfect microdisk. However, for the microdisk with an output waveguide as shown in the inset of Fig. 2(a), the mode coupling between two modes with almost the same wavelength can occur due to the break of the symmetry. Different from the mode superposition, the mode coupling will result in two new modes. A 4.5-μm-diameter microdisk surrounded by air with the refractive index of 3.2 and a 0.6-μm-wide output waveguide is simulated by finite-difference time-domain (FDTD) technique [14]. The uniform mesh cell size of 10 nm and the time step of Courant limit are used in the simulation. A cosine impulse modulated by a Gaussian function $P(x_0, y_0, t) = \exp[-(t-t_0)^2 / t_w^2]\cos(2\pi ft)$ is used as an exciting source, where t_0 and t_w are the times of the pulse center and the pulse half width, respectively, and f is the center frequency of the pulse. Symmetric or antisymmetric exciting sources relative to the center line of the output waveguide are used to simulate the modes of different symmetry independently. The perfect matched layer (PML) absorbing boundary condition is used as the boundaries to terminate the FDTD computation window. 2^{18}-step FDTD simulation is performed with an impulse at f = 200THz, $t_w = 2^9 \Delta t$, and $t_0 = 3t_w$, and the time variation of field is recorded as a FDTD output. The Padé approximation with Baker's algorithm [15] is used to transform the last 2^{15}-step FDTD output from the time-domain to the frequency-domain.

The obtained intensity spectra for TM modes are plotted in Fig. 2(a) as the red and blue lines for the symmetric and antisymmetric modes relative to the x-axis, respectively. The intensity spectrum for TM modes in the corresponding microdisk without the output waveguide is also calculated and plotted in Fig. 2(b) with the detail of spectrum from 1490 to 1490.4 nm in the inset. The modes with wavelength difference less than 5 nm are marked by circles in Fig. 2(b), which result in the coupled modes in Fig. 2(a). All of the WGMs with radial mode number $v < 4$ appear in the spectrum of Fig. 2(b), and their Q factors are larger than 10^4. However, only the coupled modes can keep high Q factors in the microdisk with the output waveguide and appear in Fig. 2(a). The Q factors of 9.1×10^3 and 2.8×10^4 are obtained for the symmetric and antisymmetric modes at the wavelength of 1490 nm in Fig. 2(a), which correspond to the coupled modes between $TM_{18,3}$ and $TM_{15,4}$ with the wavelength difference of 0.1 nm in the perfect microdisk. Two-mode competition for the symmetry and antisymmetry modes can be applied to realize optical bistability [16]. The peaks at 1433 nm and 1552 nm in Fig. 2(a) have the Q factors from 1.7×10^3 to 3×10^3, which correspond to the coupled modes between $TM_{17,3}$ and $TM_{14,4}$, and $TM_{19,3}$ and $TM_{16,4}$, respectively. The mode wavelength differences between $TM_{17,3}$ and $TM_{14,4}$, and $TM_{19,3}$ and $TM_{16,4}$ in the perfect microdisk are 2.9 and 2.6 nm, respectively, which is larger than that between $TM_{18,3}$ and $TM_{15,4}$. The Q factors of 6.5×10^2 and 1.1×10^3 are obtained for the symmetric and

antisymmetric modes at the wavelength of 1576 nm, which correspond to the coupled modes between $TM_{20,2}$ and $TM_{11,5}$ with the wavelength difference of 4.4 nm in the perfect microdisk. The Q factor of $TM_{11,5}$ is less than 10^3, thus $TM_{11,5}$ does not appear as a peak in Fig. 2(b).

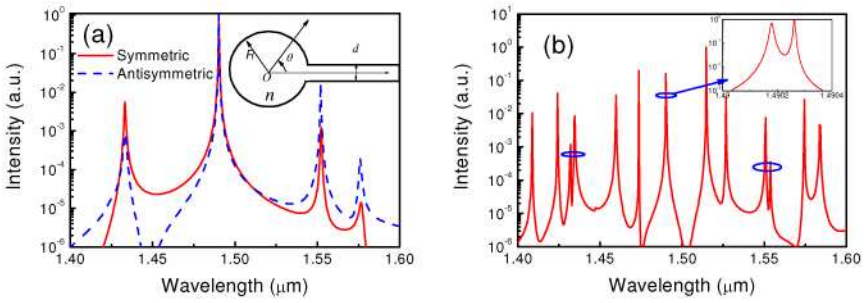

Fig. 2. The intensity spectra for TM modes obtained by FDTD simulation and Padé approximation for the 4.5-μm-diameter microdisk (a) with a 0.6-μm-wide output waveguide and (b) without the output waveguide, the circles mark the modes for coupling.

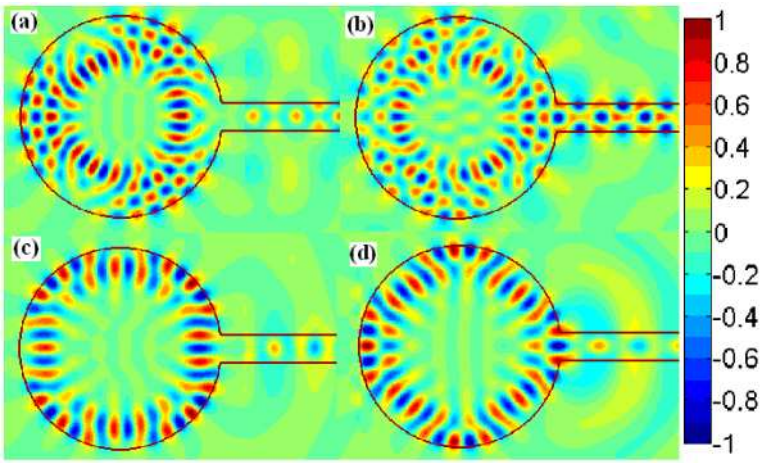

Fig. 3. The field distributions of the (a) high Q and (b) low Q TM coupled modes at wavelength of 1490 nm, and the (c) high Q and (d) low Q TM coupled mode at wavelength of 1786 nm in the 4.5-μm-diameter microdisk with a 0.6-μm-wide output waveguide. The field at the right side output waveguide is magnified 5 times for high Q coupled modes in (a) and (c).

Using a long optical pulse with a very narrow bandwidth, we can excite the mode field distribution for a single mode by the FDTD simulation. The electric field distributions of the symmetric TM coupled modes are plotted in Figs. 3(a) for the high Q and 3(b) for the low Q modes at the wavelength of 1490 nm, and 3(c) for the high Q and 3(d) for the low Q modes at the wavelength of 1786 nm, with equilateral-triangular and square mode field patterns, respectively. The mode field patterns in Figs. 3(a) and 3(b) are similar to the superposition field patterns in Figs. 1(a) and 1(b), respectively. The Q factor of the coupled mode in Fig. 3(c) at 1786 nm is 2.4×10^4, corresponding to the mode coupling between $TM_{21,1}$ and $TM_{17,2}$ with the wavelength difference of 1.4 nm. An output waveguide connected to a microdisk usually greatly reduces the Q factors of the WGMs. However, mode coupling between the WGMs results in the deformed mode field patterns as shown in Figs. 3(a) and 3(c), which can have high Q factors in the microdisk resonator with an output waveguide. It should be noted that the field patterns of Fig. 3(b) and 3(d) are obtained under exciting sources with special distributions. The corresponding mode fields disappear as soon as the exciting sources vanish.

4. Output efficiency for a coupled mode

The Q factors obtained by the FDTD simulation can be expressed as $1/Q = 1/Q_r + 1/Q_c$ with Q_r and Q_c related to a radiation loss and an output coupling loss, respectively. The output coupling loss is contributed to the directional emission in the output waveguide. However, mode Q factor will be limited by material absorption coefficient α as $Q_0 = n_g k_0/\alpha$ in a practical microcavity. At the wavelength of 1500 nm and the mode group index $n_g = 3.6$, we have $Q_0 = 1.5\times10^5$ and 1.5×10^4 as the absorption $\alpha = 1$ and 10 cm^{-1}, respectively. The output coupling efficiency of microcavity lasers can be expressed as $Q_c^{-1}/(Q^{-1} + Q_0^{-1})$. As Q is much smaller than Q_0, we have the output coupling efficiency as Q/Q_c, which can be calculated as the ratio of the energy flux through the output waveguide to the total emission energy flux of the resonator by the FDTD simulation.

The mode Q factors and the output efficiencies versus the width of the output waveguide are plotted in Figs. 4(a) for symmetric and 4(b) for antisymmetric coupled modes in the 4.5-μm-diameter microdisk. Two coupled modes are marked by symbols S (short wavelength) and L (long wavelength) according their mode wavelengths. As the width of the output waveguide is zero, the L and S coupled modes are corresponding to $TM_{18,3}$ and $TM_{15,4}$ with the wavelengths of 1489.5 and 1489.4 nm, respectively, in the perfect microdisk. But the Q factor 5.4×10^5 for the L mode obtained by FDTD simulation is of the order of a hundredth of that obtained by Eq. (1) for $TM_{18,3}$, and the Q factor of the S mode has the same value as that of $TM_{15,4}$, as the width of the output waveguide is zero. In fact, we can get exact value of Q factor less than 10^5 by the numerical simulation with the mesh cell size of 10 nm and single precision numbers. The L coupled modes have the field distributions similar to Fig. 3(b), which strong couples with the output waveguide. Similarly, standing modes forming by clockwise and anticlockwise modes with the same order [17] have uniform envelop of the field pattern along the perimeter of the microdisk and low Q factor due to strong coupling with the output waveguide. The highest output coupling efficiency is about 0.65 in Fig. 4, which can be enhanced by surrounding the microdisk laterally with insulator SiO_2 and p-electrode Au layers [18]. The output coupling efficiency is also affected by a vertical radiation loss, which is not included in the 2D FDTD simulation. However, vertical radiation loss is almost zero for TM WGMs in a cylinder resonator with a vertical semiconductor waveguiding [19].

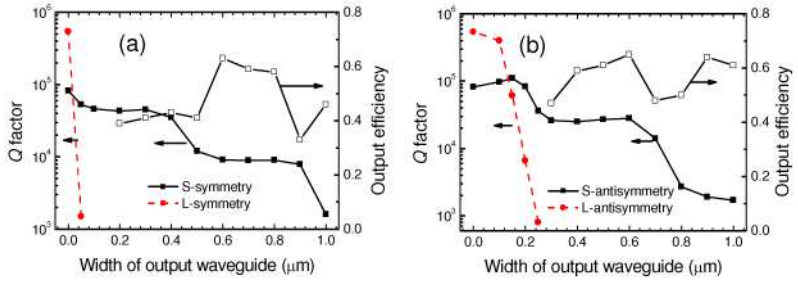

Fig. 4. Mode Q factors and output coupling efficiencies versus the width of the output waveguide for (a) symmetric and (b) antisymmetric coupling modes in the 4.5-μm-diameter microdisk, where symbols S and L mark the coupling modes with short and long wavelengths around 1490 nm.

5. Mode coupling for TE modes in a microdisk with an output waveguide

Finally, to verify the general of the above results, we also simulate the TE modes for the microdisk with an output waveguide. The intensity spectra are calculated by FDTD technique and Padé approximation with the same condition as TM modes. For a 5-μm-diameter microdisk with a 0.8-μm-wide output waveguide, the obtained intensity spectra are plotted in Fig. 5(a) as the red and blue lines for the symmetric and antisymmetric modes relative to the x-axis, respectively. The intensity spectrum for TE modes in the corresponding microdisk

without the output waveguide is also calculated and plotted in Fig. 5(b), with the modes with wavelength difference less than 5 nm marked by circles. There are many WGMs with radial mode number $v < 4$ appear in Fig. 5(b). Similar to TM modes, only the coupled modes, which induce by the mode coupling between two modes with almost the same wavelength, can keep high Q factors in the microdisk with the output waveguide and appear in Fig. 5(a).

The mode Q factors of 3.5×10^3 and 8.6×10^3 are obtained for the symmetric and antisymmetric modes at the wavelength of 1490 nm in Fig. 5(a), which correspond to the coupled modes between $TE_{28,1}$ and $TE_{20,3}$. The peaks at 1443 nm and 1542 nm in Fig. 5(a) correspond to the coupled modes between $TE_{29,1}$ and $TE_{21,3}$, and $TE_{19,3}$ and $TE_{16,4}$, respectively, and have the Q factors from 1.6×10^3 to 4.3×10^3. In Fig. 5(b), we have $TE_{17,4}$ with mode wavelength near 1490 nm besides $TE_{28,1}$ and $TE_{20,3}$. The coupled modes between $TE_{28,1}$ and $TE_{17,4}$ can have a Q factor of 10^3 when the width of the output waveguide is 0.6 μm, but do not appear in the intensity spectra of Fig. 5(a) as the width of the output waveguide is 0.8 μm. Similar to TM modes, the TE WGMs without mode coupling have a very small Q factor and do not appear in Fig. 5(a).

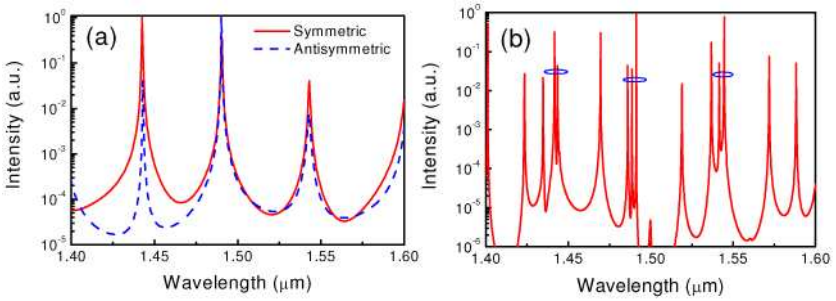

Fig. 5. The spectra of TE modes obtained by FDTD simulation and Padé approximation for a 5 μm diameter microdisk (a) with a 0.8-μm-wide output waveguide and (b) without the output waveguide, the circles mark the modes for coupling.

6. Summary

We have investigated the mode characteristics for the 2D microdisk with an output waveguide by FDTD technique. High Q modes with high output efficiency are expected due to the mode coupling between WGMs with a small wavelength difference for both TM and TE modes. The results show that the microdisk with an output waveguide can be applied to realize single mode directional emission microlasers, which is a suitable light source for photonic integrated circuits.

Acknowledgments

This work was supported by the National Nature Science Foundation of China under Grants 60777028, 60723002 and 60838003, and the Major State Basic Research Program under Grant 2006CB302804, and the Project of National Lab for Tsinghua Information Technologies.